

Article

Analysis of Iron Anchor Diseases Unearthed from Gudu Ruins in Xianyang City, Shaanxi Province, China

Bingjie Mai ¹, Youlu Chen ², Ying Zhang ¹, Yongsheng Huang ², Juanli Wang ^{1,*}, Yuhu Li ^{1,*}, Ming Cao ^{3,*} and Jing Cao ^{1,*}

¹ Ministry of Education, Engineering Research Center of Historical and Cultural Heritage Protection, School of Materials Science and Engineering, Shaanxi Normal University, Xi'an 710119, China; maibingjie@snnu.edu.cn (B.M.); y26932022@163.com (Y.Z.)

² Cultural Relics Restoration Department, Xianyang Museum, Xianyang 712000, China; skycyl666@163.com (Y.C.); huangyongsheng69@163.com (Y.H.)

³ Cultural Property Protection Center, Ningbo University of Finance & Economics, Ningbo 315175, China

* Correspondence: wangjuanli@snnu.edu.cn (J.W.); liyuhu@snnu.edu.cn (Y.L.); mcao1123@163.com (M.C.); jingcao@snnu.edu.cn (J.C.)

Abstract: Iron cultural relics are easily affected by environmental factors and can completely rust away. As early as the Qin Dynasty in ancient China, Xianyang Gudu was part of the most important transportation route to the West from ancient Chang'an; research into Xianyang Gudu has provided important information for understanding the historical changes in ancient China, East–West trade, and ancient boating technology. In this research, we use the iron anchors unearthed from the Gudu ruins in Xianyang City, Shaanxi Province, China as the research object; then, we used a scanning electron microscope–energy dispersive spectrometer (SEM-EDS), a high-resolution X-ray diffractometer (XRD), ion chromatography, and other methods to detect the corroded products of the iron anchors, and analyzed the iron anchor diseases in different preservation environments to explore the relationship between iron anchor disease and the preservation environment. This research found that the corroded products of the iron anchors contained the harmful tetragonal lepidocrocite (β -FeOOH) and that a high concentration of salt ions in the river channel accelerated the corrosion of the anchors; this analysis, based on the disease results, can provide a basis for the subsequent scientific restoration of iron anchors.

Keywords: iron anchor; corrosion product; iron relics; corrosion mechanism



Citation: Mai, B.; Chen, Y.; Zhang, Y.; Huang, Y.; Wang, J.; Li, Y.; Cao, M.; Cao, J. Analysis of Iron Anchor Diseases Unearthed from Gudu Ruins in Xianyang City, Shaanxi Province, China. *Coatings* **2022**, *12*, 381. <https://doi.org/10.3390/coatings12030381>

Academic Editor: Małgorzata Norek

Received: 28 January 2022

Accepted: 11 March 2022

Published: 14 March 2022

Publisher's Note: MDPI stays neutral with regard to jurisdictional claims in published maps and institutional affiliations.



Copyright: © 2022 by the authors. Licensee MDPI, Basel, Switzerland. This article is an open access article distributed under the terms and conditions of the Creative Commons Attribution (CC BY) license (<https://creativecommons.org/licenses/by/4.0/>).

1. Introduction

Cultural relics are precious due to their historical, artistic, scientific, and social value [1–3]. In 2002, when building Xianyang Lake, researchers discovered by accident the ruins of an old river embankment. After cleanup and excavation by archaeologists, stone embankments and a large number of cypress piles were found on the riverbed, as well as iron pillars, iron rings, iron anchors, and other equipment for anchoring boats inlaid on the steps. Through further research, the ruins here were found to be an ancient ferry from the Ming and Qing dynasties. The Gudu ruins are located on the north bank of the Weihe River (108.737242 E, 34.338084 N), Weicheng District, Xianyang City, Shaanxi Province, China; they are 230 m long from east to west and 7–10 m wide from north to south and occupy an area of about 2000 m². The Xianyang ancient ferry began in the Yin and Shang dynasties and prospered during the Qin and Han dynasties; it was called the “first ferry in the Qin Dynasty”. According to documented records, when the pedestrians stood at the head of the ferry bridge, they could see the majestic and magnificent palace of the Qin dynasty to the west. For thousands of years, Xianyang Gudu has been part of the main artery of the Guanzhong area in ancient China from the west to the western regions and from the south to Bashu area, and was the first stop from the west out of Chang'an and the ancient Silk

Road. From the Qin dynasty to the Qing dynasty in ancient China, Gudu played a very important role in transportation.

The discovery of the Gudu ruins in Xianyang was of great significance in the research of ancient transportation, commerce, military, literature, and urban changes, and has attracted widespread attention from all walks of life. In total, 172 pieces of ironware were unearthed at the Gudu ruins in Xianyang, including 12 iron anchors, 10 of which were preserved in situ in the exhibition hall of the excavation site at the Gudu ruins. The early on-site survey investigation of the unearthed ironware revealed that the batch and age of those unearthed ironware are different, and that the corrosion on the surface is more complicated. The soil on the surface of the ironware was not thoroughly cleaned after excavation, resulting in a large amount of dry and hard soil attached to its surface; some ironware was severely rusted, and the peelings were flaky, scaly, layered, and powdery. In addition to surface rust, some ironware also had defects such as deformation, cracking, fracture, perforation, etc. and on some of the thinner parts of the iron structure there were structural fractures due to corrosion.

The comprehensive and scientific analysis and detection of iron cultural relics and their diseases by modern analysis and detection methods are the premise for the protection and restoration of ironware. In this research, multiple analysis methods [4–16] were used to detect the unearthed iron anchor decay products, surface condensation, and harmful salts, and the material of the iron anchor was analyzed. Based on the results of the disease investigation, an experimental basis is provided for subsequent corresponding protection schemes.

2. Materials and Methods

2.1. Sampling

The samples in this experiment were seriously rusted, and the scientific analysis and the detection of components and rusty decay products were able to identify the cause of iron anchor corrosion and the degree of rust, to provide a scientific basis for subsequent protection and restoration [17–19]. First, the digital image collection of cultural relics samples was conducted and the disease map was drawn. Then, the samples were collected and the iron material and rust products were analyzed. Finally, the types of cultural relics disease were comprehensively analyzed and scientific restoration methods were put forward (Figure 1).

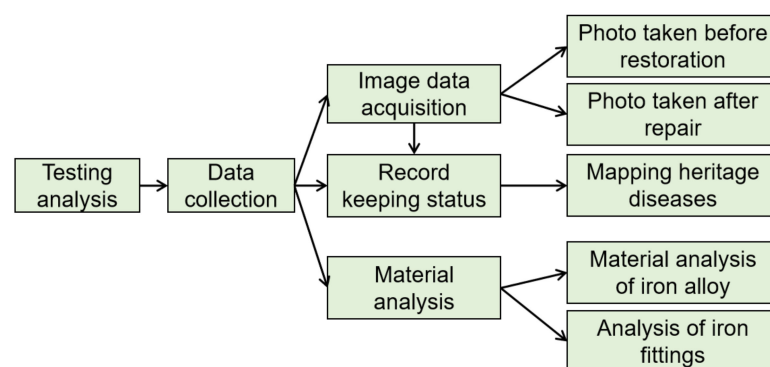


Figure 1. Flow chart describing the analysis and detection of iron relics.

2.2. Experimental Methods

Sample information: In order to ensure the maximum future and present aesthetic values of the iron anchor, this work analyzed the fallen fragments of samples from the anchor.

Ultra-depth of field optical microscopy: An ultra-depth of field optical microscope (KH-7700, Hirox Co., Ltd., Tokyo, Japan) was used to observe the macroscopic appearance of the sample; the magnification range was 20–120 times.

Metallographic analysis: the organization evaluation, process analysis, defect research and judgment of the raw materials of metal materials for processing structural parts and finished products.

SEM-EDS: SEM-EDS (SU3500, Hitachi High-Tech Co., Tokyo, Japan) was used to observe the microscopic morphology of the sample and detect the element composition and distribution. The sample was fixed on the platform with conductive adhesive, and the gold spraying time was set at 100 s to prepare the sample and eliminate the charge accumulation. The test conditions were vacuum mode, the acceleration voltage is 15 kV, and amplification was 100–300 times.

Ion chromatographic analysis: The ICS-90 ion chromatograph (Shanghai Leirui Scientific Instrument Co., Ltd, Shanghai, China) was used as the testing instrument. Grind the iron rust sample through an 80-mesh sieve, and dissolve 2 g in 100 mL of distilled water. Shake and soak for 7 days, and then detect the relevant ion content in the leachate solution. The measurement data analysis method adopted the general rules of JY/T020-1996 ion chromatography analysis method.

Laser Raman spectroscopy analysis: This analysis used the in Via Reflex micro-confocal laser Raman spectrometer (Renishaw, Gloucestershire, UK), with a scanning range of 100–4000 cm^{-1} ; the signal-to-noise ratio of the third-order peak of detection silicon was greater than 22:1; spectral resolution for the full visible spectrum was $\leq 1 \text{ cm}^{-1}$.

High-resolution X-ray diffractometer: X'Pert Pro MPD X-ray diffractometer (Smart Lab (9), Rigaku Co., Tokyo, Japan) was used as the analytical instrument; the analysis condition adopts the anode target as the copper target; the test voltage is 40 KV; the test current is 30 mA; the 2θ range is 5° – 90° ; step width, 0.02° ; scanning rate, $4^\circ/\text{min}$. The experimental data analysis method was based on “JY/T009-1996 General Principles of Rotating Target Polycrystalline X-ray Diffraction Method”; the X-ray diffraction experiment was carried out using a powder sample method, and the diffraction spectrum was analyzed by Jade 7.0.

Silver nitrate titration detection of rusty samples: Take the rusty products and grind them with agate to powder. Dissolve the sample with nitric acid. After 2 min, filter with filter paper to obtain a clear solution, then add 2–3 drops of AgNO_3 solution to the clear solution and observe whether white flocs appear. The nitric acid solution used was a dilute nitric acid solution prepared in a ratio of 2:1 to distilled water and nitric acid solution. The concentration of AgNO_3 was 1%. Observe the above reactions.

3. Results and Discussion

3.1. Investigation and Survey of the Occurrence Environment

Xianyang City, Shaanxi Province, China is located in a warm temperate zone with a continental monsoon climate; the four seasons are clearly cold, hot, dry, and wet; the climate is mild; light, heat, and water resources are abundant; the annual average precipitation is 537–650 mm; and the average temperature is 9.0 – 13.2°C . The topography of the Gudu ruins area is higher in the north and lower in the south, with a ground elevation of 378.0–397.5 m; the landform is a river valley accumulation landform. The south of the Gudu ruins relies on Xianyang Lake, the normal water level of the lake is 382.5 m, and the elevation of the Gudu ruins pit is lower than the water level of Xianyang Lake. The humidity in the ruins is above 70%. The Gudu site is a specific place formed by wading through the river with boats in early civilization to transport people and objects to the opposite bank (Figure 2). After arriving at the destination, the anchor can fix and stabilize the position of the boat. During the use of the iron anchor in the riverway water environment, the iron anchor was corroded by various ions, and the desalination protection treatment was not carried out in time after the excavation; thus, some of the iron anchors left at the excavation site contacted with the sand and salt. At the same time, the ruins relied on Xianyang Lake, and the water level of the lake changed, which caused some seepage in the ruins pit. The various chemical components contained in the seepage water made the disease more serious. Another part of the ironware is placed in the environment of the exhibition hall,

and the temperature and humidity of the exhibition hall are greatly affected by weather changes; the ironware is mixed with other types of cultural relics, and the preservation environment is relatively harsh.

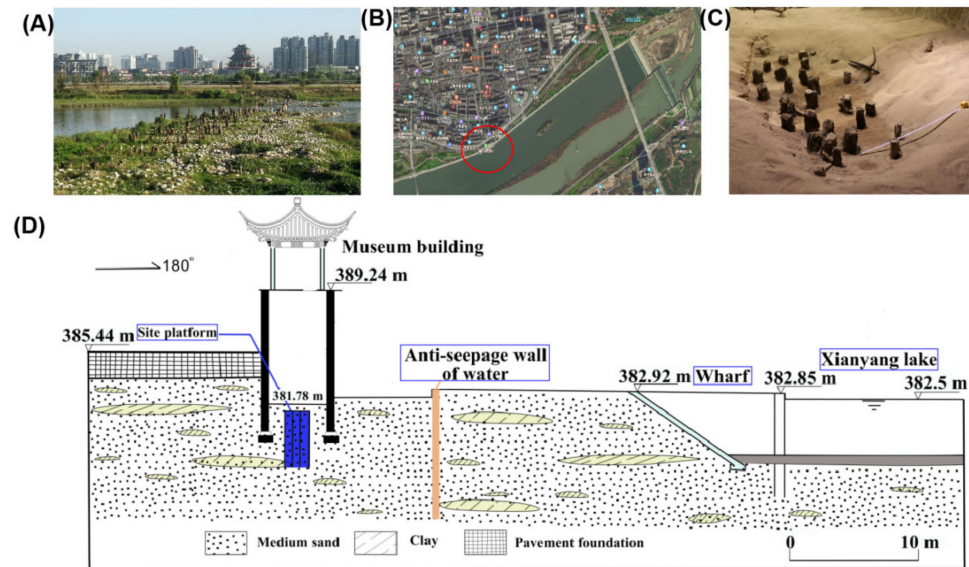


Figure 2. Occurrence conditions of Gudu ruins. (A): excavated photos of the Gudu ruins; (B): geomorphology around the Gudu ruins; (C): site photos of the Gudu ruins; (D): geological section of Gudu ruins area.

3.2. Preservation Status and Disease Type

The unearthed anchor ironware is stored in the exhibition hall of the Gudu ruins excavation site; the rest are displayed in the cultural relics exhibition hall of Xianyang Museum. The preservation conditions in the exhibition hall are simple and the ventilation equipment cannot be used for 24 h, which causes the exhibition hall humidity and temperature during the rainy season to be maintained at a high level. The on-site survey and investigation found that 91% of the ironware in this batch had different degrees of rust; 56% had severe rust, 21% had cracks and deformations, and 12% had severe damage. In total, 12 iron anchors were unearthed from the Gudu ruins and 10 iron anchors were preserved in situ in the ruins pit and the remaining iron anchors are located in the exhibition hall of the Gudu Museum. Due to various factors in the riverway environment, the iron anchors were corroded by chloride ions, and severe corrosion occurred; after unearthing, the desalination protection treatment was not carried out in time, and the chlorine in the ironware and the water and oxygen in the air further reacted with the iron, accelerating the corrosion of the ironware. At the same time, we drew the disease map of this batch of anchors. Four randomly selected anchors showed similar defects, including corrosion, iron tumor, soil attachments, welding marks, and layer stripping, as shown in Figure 3A–D.

3.3. Cast Iron Material Composition of Iron Anchor

Through metallographic examination, scanning electron microscopy (Figure 4A,B), and energy spectrum analysis (Figure 4C), the metallographic structure of the iron anchor corrosion sample was determined as ferrite with a small amount of massive cementite. This illustrates that the cast iron material of this batch of iron anchors is white iron.

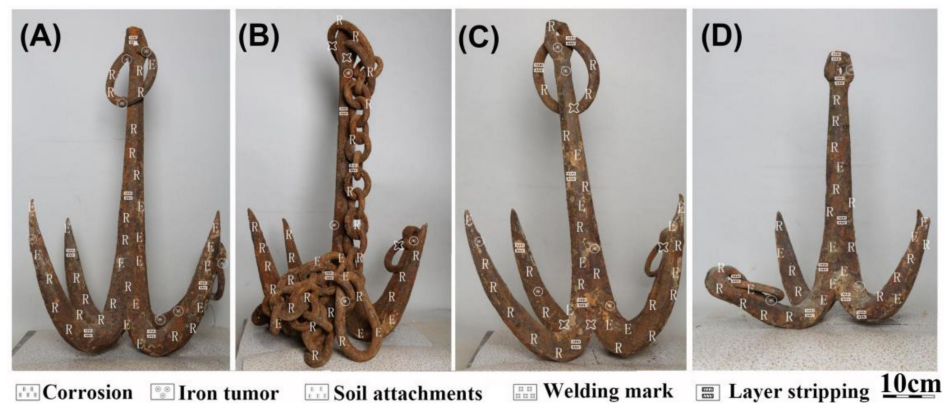


Figure 3. Typical diseases of the anchors: (A–D) are disease maps of four samples.

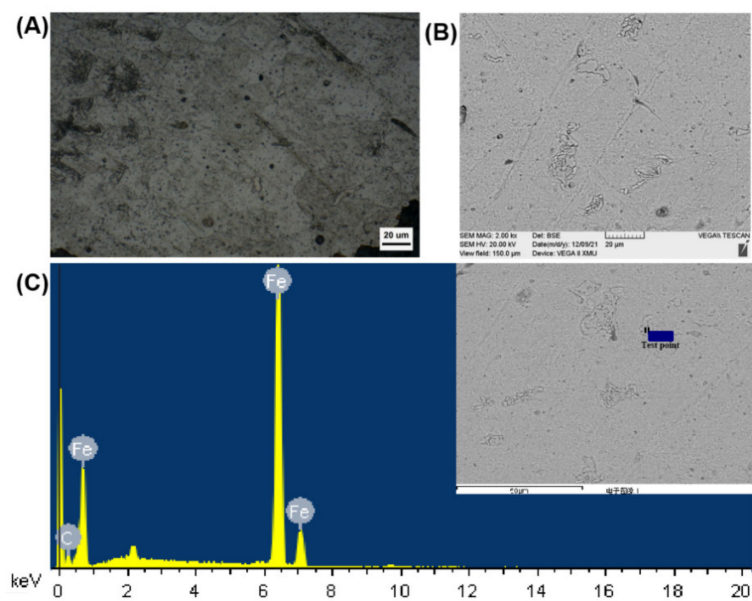


Figure 4. Metallographic analysis of iron anchor samples. (A) Metallographic microscopy characterizes the properties of metals; (B) scanning metallography of anchor; (C) EDX energy spectrum of anchor.

3.4. Corroded Microstructure

As shown in the Figure 5, there were some soil and loose rusty products on the surface of the iron anchor. A low density of rusty products on the surface of the iron anchor was observed, and an oxide film that can effectively protect the body was not formed on the surface of the iron (Figure 5A). There was rust and peeling on the surface of the iron anchor, and there are yellow rust and rusty spots, which are presumed to be the surface corroded products caused by the presence of soluble chloride salts in the sample (Figure 5B). As shown in Figure 5C, the appearance of the sample surface corrosion products is flaky, and the surface corrosion products were tan, presumably because the iron surface chloride soluble salt reacted with the iron surface generated by the brown rust products; in the subsequent experiments on the samples of chloride corrosion products and titration analysis, types of chloride and chloride content were identified. There are soil adhesion and yellow–brown rusty products on the surface of the sample iron anchor in Figure 5D, from which it can be inferred that it may be because the unearthed area of the sample is an ancient riverbed area, and some river sand residues are attached to its surface. Due to the abundant groundwater around the excavated area, the leaching effect of groundwater on the surrounding rock formations results in a high content of soluble chloride salts in

the soil around the riverbed, leading to the formation of chemical corrosion on the surface iron anchors.

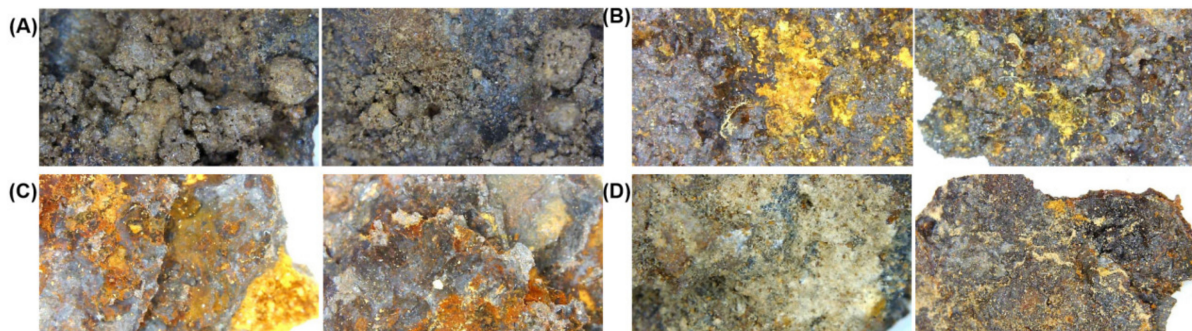


Figure 5. Iron anchor photomicrograph. (A–D) are four sample micrographs.

The scanning electron micrographs show that the microscopic morphology of the rusty products in the samples is different; the corrosion products on the surface of the samples are lumpy (Figure 6A), granular (Figure 6B), needle-like (Figure 6C), and spherical (Figure 6D), all of which have loose surface structures. This may be due to the different elemental composition of the sample iron and the different surface storage environment. The oxide layer formed on the surface has a low density, and the existence of a large number of holes means that it cannot effectively cover the inner layer, nor can it prevent further corrosion caused by the infiltration of O_2 , H_2O and Cl^- , which leads to the deterioration of the surface of the iron anchor.

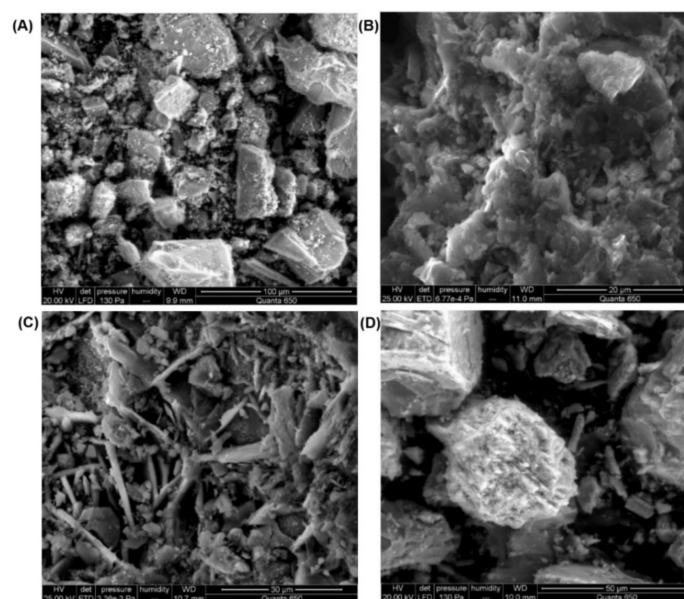


Figure 6. Electron microscope image of corrosion products of iron anchor block. (A–D) are four sample micrographs. (A) Bulk corrosion products; (B) granular corrosion products; (C) needle-like corrosion products; (D) spherical corrosion products.

3.5. Corrosion Products

The EDX energy spectrum analysis showed that the main components were silicon dioxide (Figure 7A), ferric oxide (Figure 7B), ferric oxide (Figure 7C), ferrous oxide, and calcium and magnesium carbonate (Figure 7D). Under the buried environment of river channels, silicon dioxide, calcium and magnesium carbonate appeared on iron anchors. Elemental iron is not very reductive, but in the presence of Fe, it is rapidly oxidized from a zero-valent state to a high-valence state. The corrosion of iron is a continuous process. First,

iron loses two electrons to become Fe^{2+} , and the main reactions are hydrogen evolution corrosion or oxygen absorption corrosion. We found that the soil pH ranged from 6.13 to 6.38 from sampling soil sand and gravel from Gudu ruins. When the iron is immersed in water or there is a layer of acidic water film on the surface, Fe is more active than H^+ , and the substitution reaction will occur to form Fe^{2+} and H_2 . The main Fe^{2+} compounds were ferrous oxide and ferrous hydroxide, which continue to react with oxidizing substances to form Fe_3O_4 , Fe_2O_3 , and iron hydroxide [20–22]. Consequently, we detected Fe_2O_3 , FeO_3 and FeO on the corroded surface of the anchor.

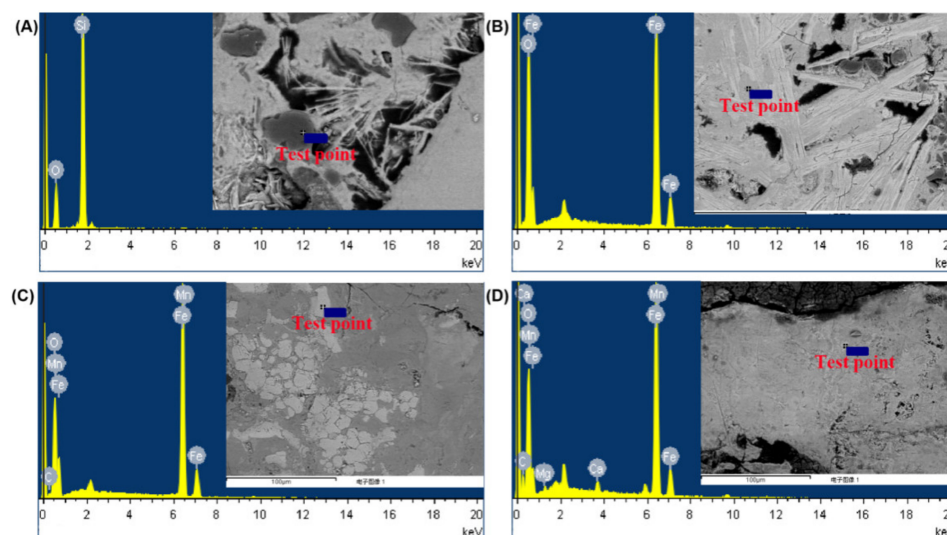


Figure 7. EDX spectrum. The iron anchor samples detected silica (A), ferric oxide (B), ferric oxide (C), and ferrous oxide and calcium–magnesium carbonate (D).

In Figure 8A, the actual peak positions on the diffraction pattern were: 21.2° , 26.6° and 36.7° , corresponding to the α -FeOOH and γ -FeOOH peak positions in the standard library, which indicated that the sample contains goethite (α -FeOOH) and lepidocrocite (γ -FeOOH); 27.1° and 50.4° , corresponding to the silica peak positions in the standard library, which indicated that the sample contains silica; 39.9° and 54.2° , corresponding to the peak positions of γ - Fe_2O_3 in the standard library, which indicated that the sample contains γ - Fe_2O_3 ; 43.1° , corresponding to the peak positions of Fe_3O_4 in the standard library, which indicated that the sample contains Fe_3O_4 . As shown Figure 8B, the peak locations at 21.2° , 26.6° , and 36.7° indicated that the sample contains α -FeOOH and γ -FeOOH; 50.4° , corresponding to the silica peak positions in the standard library, which indicated that the sample contains silica; 39.9° and 54.2° , corresponding to the peak positions of γ - Fe_2O_3 in the standard library, which indicated that the sample contains γ - Fe_2O_3 . The peak locations at 21.2° and 26.6° in Figure 8C indicated that the sample contains α -FeOOH and γ -FeOOH. Figure 8C showed a characteristic peak in 44.7° of silica. In Figure 8D, the actual peak positions on the diffraction pattern were 26.6° and 43.1° , corresponding to the α -FeOOH peak positions in the standard library, which indicated that the sample contains goethite (α -FeOOH). Figure 8D also showed a characteristic peak of silica, similar to Figure 8C. From the above four typical samples, it can be seen that the rusty product samples of the sampled iron anchors contain goethite (α -FeOOH), hematite (α - Fe_2O_3), maghemite (γ - Fe_2O_3), akaganeite (β -FeOOH), lepidocrocite (γ -FeOOH), and magnetite (Fe_3O_4), as well as a small amount of hexagonal lepidocrocite. The lepidocrocite (γ -FeOOH) is unstable and, under certain conditions, can be transformed into goethite (α -FeOOH) and magnetite (Fe_3O_4). This showed that the iron anchor corroded product samples were all the corroded products with different combinations of corrosion components and a serious degree of corrosion. Silica (SiO_2) was also detected in the sample; this substance is the main component of soil and sand, and the presence of this substance may be due to the

excavation location of the batch of ironware in the sand riverway, and a large amount of sand adhered to the surface of the unearthed ironware to form the surface pollutants and hardened materials. When cleaning, sandblasting technology and sanding machines can be used to physically remove silica.

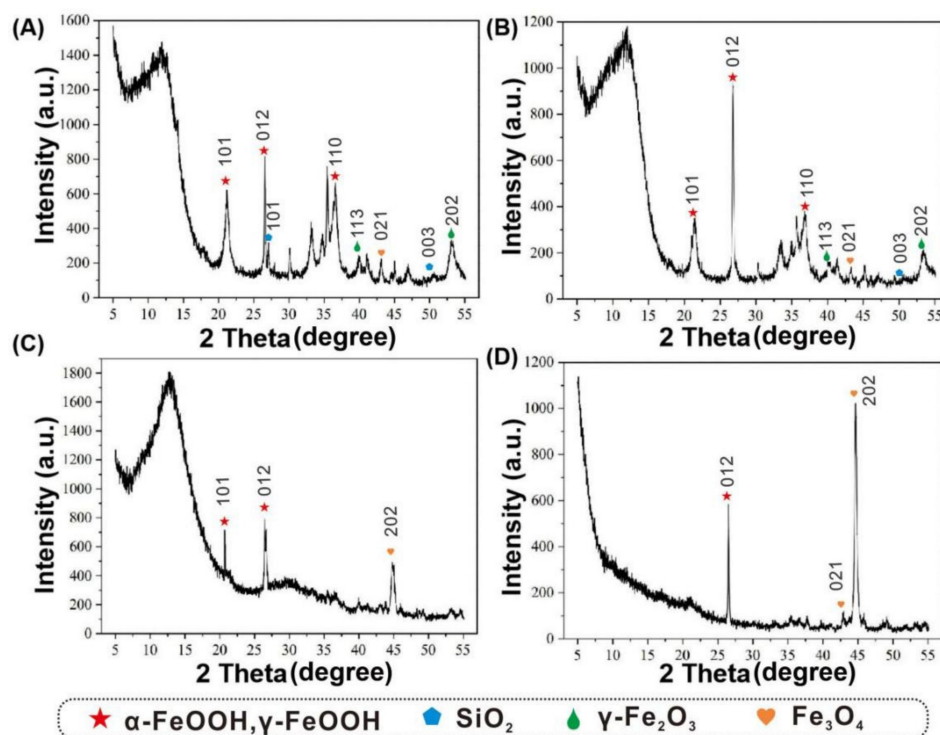


Figure 8. XRD spectrum. (A–D) XRD maps of four sample.

It can be seen from the Figure 9 that the peak at 428 cm^{-1} of samples in Figure 9A,B was consistent with the 400 cm^{-1} peak of $\alpha\text{-FeOOH}$. The peaks at 226 and 278 cm^{-1} were consistent with those at 230 and 250 cm^{-1} of $\alpha\text{-Fe}_2\text{O}_3$. Therefore, it is speculated that goethite ($\alpha\text{-FeOOH}$) and hematite ($\alpha\text{-Fe}_2\text{O}_3$) may be present in the sample. The peaks at 221 and 257 cm^{-1} in Figure 9C,D were consistent with those at 230 and 250 cm^{-1} in $\alpha\text{-Fe}_2\text{O}_3$. The peak at 240 cm^{-1} was consistent with that of $\gamma\text{-FeOOH}$ at 245 cm^{-1} , so it was speculated that the sample may contain hematite ($\alpha\text{-Fe}_2\text{O}_3$) and fibroite ($\gamma\text{-FeOOH}$). The Raman spectrum showed that the corroded products mainly contain goethite ($\alpha\text{-FeOOH}$), lepidocrocite ($\gamma\text{-FeOOH}$), and hematite ($\alpha\text{-Fe}_2\text{O}_3$), and most of the samples contain multiple substances, with clear characteristic peaks. It is shown that these samples are rusty products with different combinations of rusty components and serious degrees of rust.

3.6. Chloride Ions in the Sample

After the four samples were titrated with silver nitrate solution (Figure 10), white flocculent precipitates appeared, indicating that there were different concentrations of chloride and soluble chloride salts in the four samples, and the content of white precipitate in sample No. 2 is greater than that in other samples, confirming that sample No. 2 had a higher chloride content, as shown by the ion chromatography analysis.

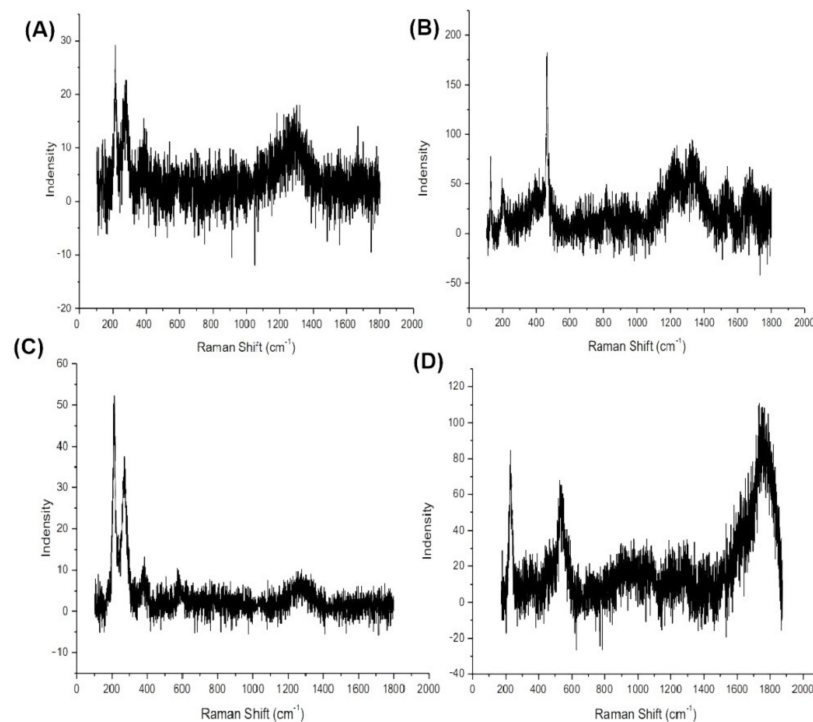


Figure 9. Raman spectrogram. (A–D) Raman maps of four sample.

Sample	Cl ⁻	NO ³⁻	SO ₄ ²⁻
1	0.018%	0.033%	0.18%
2	0.056%	0.052%	0.27%
3	0.030%	0.027%	0.20%
4	0.037%	0.027%	0.60%

Figure 10. Ion chromatography and titrating with silver nitrate solution results.

3.7. Mechanism of Corrosion Evolution

There are many reasons for iron corrosion, including uneven structure, more impurities, and the unstable properties of iron itself. In addition, the protection of iron relics is also greatly influenced and restricted by the environment [23,24]. In the corrosion process of ironware cultural relics, the chemical corrosion, electrochemical corrosion and microbial corrosion often occur at the same time on the surface of ironware [25,26].

Iron anchors unearthed at the Gudu ruins were in a state of riverway water corrosion; the chloride ions in the river water have a destructive effect on the surface oxide film and accelerate the dissolution of the surface film [27–29]. After finally sinking into the sand, the Gudu ruins were immersed in an environment rich in groundwater for a long time, causing the iron anchor to continue to react with the chloride ions in the water, which promoted the dissolution of the film surface and was destroyed.

As mentioned earlier, the soil environment of Gudu ruins was weakly acidic; when the water film in contact with the iron surface becomes acidic, the active order of iron is ahead of H⁺, and substitution reactions occur to form Fe²⁺ and H₂ [30,31]. While, Gudu ruin was located below the level of Xianyang Lake in all seasons, presenting a humid environment. In the humid environment of the buried environment, the iron cultural relics on the basis of chemical corrosion and electrochemical corrosion would also participate.

Metallurgical microscopy (Figure 4) showed the presence of ferrite and cementite on the corroded surface. When the oxygen-containing water film is formed on the surface of the iron anchor, there are a certain amount of electrolyte ions (Cl^- , Na^+), and the ferrite ($\alpha\text{-Fe}$) and cementite (Fe_3C) will form numerous microgalvanic cells, thus forming microcell corrosion. As shown in Figure 11, the electrolyte water film on the surface of the iron anchor is the external circuit, Fe is the internal anode, and Fe_3C is the cathode. Compared with the single chemical corrosion, the electrochemical reactions could greatly accelerate the corrosion of iron.

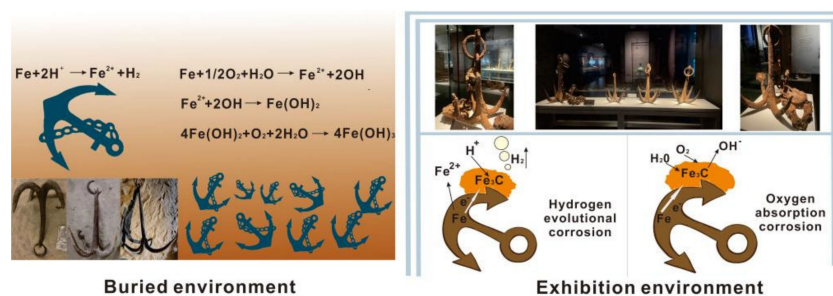


Figure 11. Corrosion mechanism of iron anchor in different environments.

Moreover, in the corrosive medium of the atmosphere, soil and water with a high salt content, especially a high chloride content, will destroy the stable $\alpha\text{-Fe}_2\text{O}_3$ oxide film on the surface of ironware, which will accelerate the corrosion of iron. In the buried environment, the main chloric corrosion product of iron cultural relics is FeCl_3 , which is concentrated in the form of an acidic solution between iron matrix and rust layer, as well as in the holes and crevices of the rust layer. When the iron relics were unearthed, FeCl_3 was oxidized and hydrolyzed in the air, producing FeOOH : $4\text{FeCl}_3 + \text{O}_2 + 6\text{H}_2\text{O} \rightarrow 4\text{FeOOH} + 8\text{HCl}$. The FeOOH produced by the reaction may be $\alpha\text{-FeOOH}$, $\beta\text{-FeOOH}$, or $\gamma\text{-FeOOH}$. This is because the chloride can accelerate local corrosion, such as pitting, stress corrosion, inter-granular corrosion, and crevice corrosion, and Cl^- could prevent the conversion of active $\gamma\text{-FeOOH}$ generated on the surface of steel to inactive $\alpha\text{-FeOOH}$ [32–34]. However, the corrosion of these anchors was not explored and further protected over time, which resulted in salt ions exacerbating the corrosion of anchors after they were unearthed.

4. Conclusions

The iron cultural relics are a type of cultural relics that are difficult to preserve in the existing cultural relics. Due to their special physical and chemical properties, they are relatively small in number and are easily rusted due to environmental factors. This research took the iron anchors unearthed from the Gudu ruins in Xianyang City, Shaanxi Province, China as the research object. The disease and corrosion mechanisms of the iron anchors unearthed were researched by XRD, EDX, Raman spectroscopy, ion chromatography, and nitrate titration, to explore the storage environment and the corrosion before and after the excavation and the change of the relationship between the storage environment and the anchor disease. The research found that iron anchors unearthed at the Gudu ruins were in a state of riverway water corrosion, and the abundant chloride ions in the river intensified the corrosion of iron anchors before they were excavated, and the Gudu ruin was located below the level of Xianyang Lake in all seasons, presenting a humid environment, which further promoted the electrochemical corrosion of iron anchors after they were excavated. However, the corrosion of these anchors was not explored or further protected over time, which resulted in salt ions aggravating the corrosion of anchors after they were unearthed, and the electrochemical reaction could greatly accelerate the corrosion of iron in the humid exhibition environment. Therefore, the subsequent protection and repair of these anchors should be derusting, desalting, and cleaning as soon as possible, to prevent acceleration of the destruction of cultural relics, and the research on the correlation between environment

and deterioration of iron relics is very important to scientifically formulate a route for protection technology.

Author Contributions: Conceptualization, B.M., J.W., M.C. and J.C.; Data curation, Y.C., Y.H. and M.C.; Formal analysis, M.C.; Funding acquisition, B.M., J.W. and J.C.; Investigation, B.M., Y.C., Y.Z. and Y.H.; Methodology, J.W., Y.L. and M.C.; Project administration, Y.L. and J.C.; Software, Y.Z.; Writing—original draft, B.M.; Writing—review & editing, J.W. and J.C. All authors have read and agreed to the published version of the manuscript.

Funding: The authors gratefully acknowledge the financial support by the National Natural Science Foundation of China (No. 22102094), the Fundamental Research Funds for the Central Universities (GK 202103061 and GK 202103058), and the Key Research and Development Program of Shaanxi Province, China (No. 2021SF-457).

Institutional Review Board Statement: Not applicable.

Informed Consent Statement: Not applicable.

Data Availability Statement: The datasets used and/or analysis results obtained in the current study are available from the corresponding author on request.

Acknowledgments: The authors thank Xianyang Museum and Xianyang Gudu Ruin Museum of China for their support and help in this project.

Conflicts of Interest: The authors declare that they have no conflict of interest related to this work. We declare that we do not have any commercial or associated interest that represents a conflict of interest in connection with the work submitted.

References

1. Song, L.; Li, X.; Yang, Y.G.; Zhu, X.; Guo, Q.; Liu, H. Structured-light based 3D reconstruction system for cultural relic packaging. *Sensors* **2018**, *18*, 2981. [[CrossRef](#)] [[PubMed](#)]
2. Li, J.; Zhang, X.; Xiao, L.; Liu, K.; Li, Y.; Zhang, Z.; Chen, Q.; Ao, X.; Liao, D.; Gu, Y.; et al. Changes in soil microbial communities at Jinsha earthen site are associated with earthen site deterioration. *BMC Microbiol.* **2020**, *20*, 147. [[CrossRef](#)] [[PubMed](#)]
3. Sun, M.; Zhang, F.; Huang, X.; Han, Y.; Jiang, N.; Cui, B.; Guo, Q.; Kong, M.; Song, L.; Pan, J. Analysis of microbial community in the archaeological ruins of Liangzhu city and study on protective materials. *Front. Microbiol.* **2020**, *11*, 684. [[CrossRef](#)]
4. Zhou, W.; Gan, Q.; Ji, J.; Yao, N.; Wang, J.; Zhou, Z.; Qi, X.; Shi, J. Non-destructive identification of pigments printed on six imperial China engraved coiling dragon stamps. *J. Raman Spectrosc.* **2016**, *47*, 316–320. [[CrossRef](#)]
5. Wang, X.; Zhen, G.; Hao, X.; Tong, T.; Ni, F.; Wang, Z.; Jia, J.; Li, L.; Tong, H. Spectroscopic investigation and comprehensive analysis of the polychrome clay sculpture of hua yan temple of the liao dynasty. *Spectrochim. Acta Part A Mol. Biomol. Spectrosc.* **2020**, *240*, 118574. [[CrossRef](#)] [[PubMed](#)]
6. Hunt, A.; Thomas, P.; James, D.; David, B.; Geneste, J.-M.; Delannoy, J.-J.; Stuart, B. The characterisation of pigments used in X-ray rock art at dalakngalarr 1, central-western arnhem land. *Microchem. J.* **2016**, *126*, 524–529. [[CrossRef](#)]
7. Ilmi, M.M.; Nurdini, N.; Maryanti, E.; Saiyasombat, C.; Setiawan, P.; Kadja, G.T.M. Ismunandar multi-analytical characterizations of prehistoric rock art pigments from karim cave, sangkulirang–mangkalihat site, east kalimantan, indonesia. *Microchem. J.* **2020**, *155*, 104738. [[CrossRef](#)]
8. Zaffino, C.; Guglielmi, V.; Faraone, S.; Vinaccia, A.; Bruni, S. Exploiting external reflection FTIR spectroscopy for the in-situ identification of pigments and binders in illuminated manuscripts. Brochantite and posnjakite as a case study. *Spectrochim. Acta Part A Mol. Biomol. Spectrosc.* **2015**, *136 Pt B*, 1076–1085. [[CrossRef](#)]
9. Fu, P.; Teri, G.; Li, J.; Huo, Y.; Yang, H.; Li, Y. Analysis of an ancient architectural painting from the jiangxue palace in the imperial museum, Beijing, China. *Anal. Lett.* **2020**, *54*, 684–697. [[CrossRef](#)]
10. Moyo, S.; Mphuthi, D.; Cukrowska, E.; Henshilwood, C.S.; van Niekerk, K.; Chimuka, L. Blombos cave: Middle stone age ochre differentiation through FTIR, ICP OES, ED XRF and XRD. *Quat. Int.* **2016**, *404*, 20–29. [[CrossRef](#)]
11. Li, J.; Mai, B.; Fu, P.; Teri, G.; Li, Y.; Cao, J.; Li, Y.; Wang, J. Multi-analytical research on the caisson painting of Dayu temple in Hancheng, Shaanxi, China. *Coatings* **2021**, *11*, 1372. [[CrossRef](#)]
12. Rosi, F.; Burnstock, A.; Berg, K.; Miliani, C.; Brunetti, B.G.; Sgamellotti, A. A non-invasive XRF study supported by multivariate statistical analysis and reflectance FTIR to assess the composition of modern painting materials. *Spectrochim. Acta Part A Mol. Biomol. Spectrosc.* **2009**, *71*, 1655–1662. [[CrossRef](#)] [[PubMed](#)]
13. Bisegna, F.; Ambrosini, D.; Paoletti, D.; Sfarra, S.; Gugliermetti, F. A qualitative method for combining thermal imprints to emerging weak points of ancient wall structures by passive infrared thermography—A case study. *J. Cult. Herit.* **2014**, *15*, 199–202. [[CrossRef](#)]

14. Kubik, M. Chapter 5 hyperspectral imaging: A new technique for the non-invasive study of artworks. In *Physical Techniques in the Study of Art, Archaeology and Cultural Heritage*; Elsevier: Amsterdam, The Netherlands, 2007; Volume 2, pp. 199–259. [[CrossRef](#)]
15. Ricci, M.; Laureti, S.; Malekmohammadi, H.; Sfarra, S.; Lanteri, L.; Colantonio, C.; Calabrò, G.; Pelosi, C. Surface and interface investigation of a 15th century wall painting using multispectral imaging and pulse-compression infrared thermography. *Coatings* **2021**, *11*, 546. [[CrossRef](#)]
16. Elias, M.; Mas, N.; Cotte, P. Review of several optical non-destructive analyses of an easel painting. Complementarity and crosschecking of the results. *J. Cult. Herit.* **2011**, *12*, 335–345. [[CrossRef](#)]
17. Tao, N.; Wang, C.; Zhang, C.; Sun, J. Quantitative measurement of cast metal relics by pulsed thermal imaging. *Quant. Infrared Thermogr. J.* **2020**, *5*, 27–40. [[CrossRef](#)]
18. Ambrosini, D.; Paoletti, A.; Paoletti, D.; Sfarra, S. NDT methods in artwork corrosion monitoring. In *O3A: Optics for Arts, Architecture, and Archaeology*; SPIE: Philadelphia, PA, USA, 2007; pp. 327–335. [[CrossRef](#)]
19. Xiaoli, L.; Ning, T.; Sun, J.G.; Yong, L.; Liang, Q.; Fei, G.; Yi, H.; Guang, W.; Lichun, F. Evaluation of an ancient cast-iron Buddha head by step-heating infrared thermography. *Infrared Phys. Technol.* **2019**, *98*, 223–229. [[CrossRef](#)]
20. Motte, R.D.; Basilico, E.; Mingant, R.; Kittel, J.; Ropital, F.; Combrade, P.; Necib, S.; Deydier, V.; Crusset, D.; Marcelin, S. A study by electrochemical impedance spectroscopy and surface analysis of corrosion product layers formed during CO₂ corrosion of low alloy steel. *Corros. Sci.* **2020**, *172*, 108666. [[CrossRef](#)]
21. Remazeilles, C.; Neff, D.; Bourdoiseau, J.A.; Sabot, R.; Jeannin, M.; Refait, P. Role of previously formed corrosion product layers on sulfide-assisted corrosion of iron archaeological artefacts in soil. *Corros. Sci.* **2017**, *129*, 169–178. [[CrossRef](#)]
22. Samide, A.; Tutunaru, B.; Dobritescu, A.; Negrila, C. Study of the corrosion products formed on carbon steel surface in hydrochloric acid solution. *J. Therm. Anal.* **2012**, *110*, 145–152. [[CrossRef](#)]
23. Tamura, H. The role of rusts in corrosion and corrosion protection of iron and steel. *Corros. Sci.* **2008**, *50*, 1872–1883. [[CrossRef](#)]
24. Novakova, A.A.; Gendler, T.S.; Manyurova, N.D.; Turishcheva, R.A. A mössbauer spectroscopy study of the corrosion products formed at an iron surface in soil. *Corros. Sci.* **1997**, *39*, 1585–1594. [[CrossRef](#)]
25. Watkinson, D.E.; Rimmer, M.B.; Emmerson, N.J. The influence of relative humidity and intrinsic chloride on post-excavation corrosion rates of archaeological wrought iron. *Stud. Conserv.* **2019**, *64*, 456–471. [[CrossRef](#)]
26. Carlin, W.; Keith, D.; Rodriguez, J. Less is more: Measure of chloride removal rate from wrought iron artifacts during electrolysis. *Stud. Conserv.* **2001**, *46*, 68–76. [[CrossRef](#)]
27. Song, Y.; Jiang, G.; Chen, Y.; Zhao, P.; Tian, Y. Effects of chloride ions on corrosion of ductile iron and carbon steel in soil environments. *Sci. Rep.* **2017**, *7*, 6865. [[CrossRef](#)]
28. Liu, T.M.; Wu, Y.H.; Luo, S.X.; Sun, C. Effect of soil compositions on the electrochemical corrosion behavior of carbon steel in simulated soil solution. *Mater. Werkst.* **2010**, *41*, 228–233. [[CrossRef](#)]
29. Chen, J.; Chen, Z.; Ai, Y.; Xiao, J.; Pan, D.; Li, W.; Huang, Z.; Wang, Y. Impact of soil composition and electrochemistry on corrosion of rock-cut slope nets along railway Lines in China. *Sci. Rep.* **2015**, *5*, 14939. [[CrossRef](#)]
30. Viereck, S.; Jovanovic, Z.R.; Haselbacher, A.; Steinfeld, A. Investigation of Na₂SO₄ removal from a supercritical aqueous solution in a dip-tube salt separator. *J. Supercrit. Fluids* **2017**, *133*, 146–155. [[CrossRef](#)]
31. Galvan-Reyes, C.; Fuentes-Aceituno, J.C.; Salinas-Rodríguez, A. The role of alkalizing agent on the manganese phosphating of a high strength steel part 1: The individual effect of naoh and NH₄OH. *Surf. Coat. Technol.* **2016**, *291*, 179–188. [[CrossRef](#)]
32. Wang, Y.; Kong, G.; Che, C.; Zhang, B. Inhibitive effect of sodium molybdate on the corrosion behavior of galvanized steel in simulated concrete pore solution. *Constr. Build. Mater.* **2018**, *162*, 383–392. [[CrossRef](#)]
33. Ge, C.Y.; Yang, X.G.; Hou, B.R. Synthesis of polyaniline nanofiber and anticorrosion property of polyaniline–epoxy composite coating for q235 steel. *J. Coat. Technol. Res.* **2012**, *9*, 59–69. [[CrossRef](#)]
34. Ye, Y.; Liu, Z.; Liu, W.; Zhang, D.; Zhao, H.; Wang, L.; Li, X. Superhydrophobic oligoaniline-containing electroactive silica coating as pre-process coating for corrosion protection of carbon steel. *Chem. Eng. J.* **2018**, *348*, 940–951. [[CrossRef](#)]